中國機械工程學刊第三十九卷第四期第 375~384 頁(民國一百零七年)
Journal of the Chinese Society of Mechanical Engineers, Vol.39, No.4, pp 375~384 (2018)

Fault Feature Enhancement of Rolling Bearings Based on Singular Spectrum Decomposition

Chun-Hong Dou*, Xue-Ye Wei**, Jun-Hong Zhang* and Liang Hu*

Keywords：singular spectrum decomposition (SSD), feature enhancement, fault diagnosis, condition monitoring, rolling bearing.

ABSTRACT

Weak fault information features regularly in a defective rolling bearing. Consequently, fault diagnosis of rolling bearings is always challenging. Based on stationarity and linearity, traditional methods for data analysis are scarcely suitable for processing bearing fault data. Although applied to investigate nonstationary and nonlinear data, either of EMD and EEMD faces mode mixing. For overcoming the shortcoming, this paper introduced singular spectrum decomposition (SSD), a new method for analyzing nonstationary and nonlinear data, to examine bearing fault data and then proposed a novel method for fault feature enhancement of bearings based on SSD. Afterwards, the performance of the proposed method was benchmarked against each of envelope analysis, EMD and EEMD numerically and experimentally. Thus, the comparison indicates that SSD outperforms the other methods in retrieving physically interpretative components as a result of restraining mode mixing. Therefore, the proposed method demonstrates the potential for enhancing fault features of bearings.

INTRODUCTION

Rolling bearings have demonstrated wide application in various industrial fields. A rolling bearing generally shoulders complex loads and works in unsteady conditions. For this reason, vibrations of a defective rolling bearing typically exhibit nonstationary and nonlinear properties. Aiming at deciphering stationary and linear data, some traditional techniques for data processing, such as statistical parameters and Fourier transform, seem scarcely suitable for analyzing bearing fault data (Huang, N.E., Shen, Z., Long, S.R., Wu, M.L.C., Shih, H.H., Zheng, Q.N., Yen, N.C., Tung, C.C. and Liu, H.H., 1998). In addition, wavelet transform (WT) has been proposed to investigate nonstationary data (Daubechies, I., 1992). Nevertheless, the WT usually lacks adaption for the investigated data (Huang, N.E., Shen, Z., Long, S.R., Wu, M.L.C., Shih, H.H., Zheng, Q.N., Yen, N.C., Tung, C.C. and Liu, H.H., 1998). In recent decades, empirical mode decomposition (EMD) has been put forward for studying nonstationary and nonlinear data and achieved some good results (Huang, N.E., Shen, Z., Long, S.R., Wu, M.L.C., Shih, H.H., Zheng, Q.N., Yen, N.C., Tung, C.C. and Liu, H.H., 1998). However, EMD frequently suffers from mode mixing, which means that either a single component contains different time scales or similar time scales reside in different components (Wu, Z.H. and Huang, N.E., 2009). Consequently, this normally makes physical meaning of an individual component unclear (Wu, Z.H. and Huang, N.E., 2009). For remedying this drawback, ensemble empirical mode decomposition (EEMD), an improved version of EMD, was developed (Wu, Z.H. and Huang, N.E., 2009). The fundamental principle of EEMD is firstly to project different portions of an original data onto the corresponding time-frequency grids provided by added white noise and then to cancel the added white noise by ensemble averaging of components from different trials. Nevertheless, it seems intractable to determine amplitude of the added white noise as well as to select a proper ensemble number due to lacking a practical guideline (Zhang, J., Yan, R., Gao, R.X. and Feng, Z., 2010; Lin, J., 2012). As a result, a strong need exists to develop some novel techniques for analysis of bearing vibration data.

In past decades, singular spectrum analysis (SSA), as an adaptive nonparametric spectral estimation method, has been employed for analyzing short and noisy data (Vautard, R. and Ghil, M., 1989; Vautard, R., Yiou, P. and Ghil, M., 1992). SSA has an advantage over other methods for data analysis in enhancing periodic contents of original data and

Paper Received September, 2016. Revised May, 2017. Accepted August, 2017. Author for Correspondence: Chun-Hong Dou.

* *Graduate Student, School of Electronic and Information Engineering, Beijing Jiaotong University, No. 3 Shangyuancun, Haidian District, Beijing 100044, P. R. China.*

** *Professor, School of Electronic and Information Engineering, Beijing Jiaotong University, No. 3 Shangyuancun, Haidian District, Beijing 100044, P. R. China.*

retrieving a highly non-harmonic oscillation buried in original data (Vautard, R. and Ghil, M., 1989; Vautard, R., Yiou, P. and Ghil, M., 1992). In general, the use of SSA may make extracted components from complex data physically interpretative (Vautard, R. and Ghil, M., 1989; Vautard, R., Yiou, P. and Ghil, M., 1992). Unfortunately, SSA is still hardly automatic for determining the window length (or the embedding dimension) and selecting the principal components for reconstruction of a specific series. To resolve this problem, singular spectrum decomposition (SSD), an iterative SSA-based method, was presented (Bonizzi, P., KAREL, J.M., Meste, O. and Peeters, R.L., 2014). Different from SSA, SSD can determine the embedding dimension and choose the principal components for reconstruction fully automatically (Bonizzi, P., KAREL, J.M., Meste, O. and Peeters, R.L., 2014). By additional wrapping-around, SSD can enhance oscillatory contents in original data. In addition, SSD can guarantee energy of the residual to be decreased iteratively. Hence, SSD demonstrates the potential for restraining mode mixing and for separating intermittent components at transition points accurately. Currently, SSD has been successfully applied to data analysis in biological and physical disciplines (Bonizzi, P., KAREL, J.M., Meste, O. and Peeters, R.L., 2014).

This paper introduced SSD to explore bearing vibration data and proposed a novel method for fault feature enhancement based on SSD. Afterwards, the performance of the proposed method was benchmarked against each of envelope analysis, EMD and EEMD numerically and experimentally. The results show that SSD outperforms each of the other methods in enhancing fault features of bearings.

SINGULAR SPECTRUM DECOMPOSITION (SSD)

SSD can decompose an original signal into a collection of physically-interpretative narrow-banded components iteratively. For automatically setting fundamental parameters, SSD was devised elaborately. SSD comprises three steps: embedding, decomposition and reconstruction. The SSD process for the time series $x(n)$ $(n=1,2,\cdots,N)$ is formulated as follows.

Embedding: Choice of the Embedding Dimension

SSD automatically determines the embedding dimension M at iteration j as follows.

(1) Calculate the Power Spectral Density (PSD) of the residual time series at iteration j, $v_j(t)=x(n)-\sum_{k=1}^{j-1} v_k(n)$, $\left(v_0(n)=x(n)\right)$. Then, estimate the primary frequency $f_{\max}$ for the dominant peak of the PSD.

(2) At the first iteration, testing for a sizable trend is conducted. If the normalized frequency $f_{\max}/F_s$ is less than a preset threshold (usually 0.001), where the parameters F_s represents the sample frequency, there exists a sizable trend in the residual. Here, the embedding dimension is typically set as $M=\frac{N}{3}$, according to an existing work (Vautard, R., Yiou, P. and Ghil, M., 1992).

(3) For iteration $j>1$, the embedding dimension is selected to $M=1.2\frac{F_s}{f_{\max}}$. Here, the margin 20% of a time span aims to increase identification accuracy of SSA.

Embedding: Building of Trajectory Matrix by Wrapping-around

With the embedding dimension M, the original series $x(n)$ is transformed into an $(M\times N)$ matrix X, where the i^{th} row is defined as $x_i=\left[x(i),...,x(N),x(1),...,x(i-1)\right]$, $i=1,...,M$. Accordingly, the matrix X can be written as $X=[x_1{}^T,x_2{}^T,\cdots,x_M{}^T]^T$. For example, given the time series $x(n)=\{1,2,3,4,5\}$ and the embedding dimension $M=3$, the corresponding trajectory matrix is

$$X=\left[\begin{array}{ccc|cc} 1 & 2 & 3 & 4 & 5 \\ 2 & 3 & 4 & 5 & 1 \\ 3 & 4 & 5 & 1 & 2 \end{array}\right]. \tag{1}$$

Here, the block at the left-hand side stands for the trajectory matrix defined in the standard SSA. As shown in Equation (1), the alternative matrix wraps around the time series $x(n)$. Thus, SSD seemingly has an advantage over the SSA method in enhancing oscillatory information and supplying essential characteristics for the decrease of energy of the residual.

In addition, for performing the average along the i^{th} cross-diagonal of X, SSD moves the wrapped part of the right-hand block in Eq. (1) to the top right of the left-hand block so that each cross-diagonal of the appended matrix X contains the same number of element M. For the previous example,

$$X=\left[\begin{array}{ccc|cc} & & 1 & & \\ & 1 & 2 & & \\ 1 & 2 & 3 & 4 & 5 \\ 2 & 3 & 4 & 5 & * \\ 3 & 4 & 5 & * & * \end{array}\right], \tag{2}$$

where the asterisks indicate left vacancies after the wrapped part is moved to the top right of the left-hand block.

Decomposition

In this step, the singular value decomposition of the trajectory matrix X is implemented, $X = UDV^T$. Here, $U_{M\times M}$ and $V_{K\times K}$ denote orthogonal matrices containing the left and the right singular vectors, respectively, and $D_{M\times K}$ is a diagonal matrix with the singular value σ_i on the principal diagonal, where $\sigma_i = \sqrt{K\lambda_i}$ with λ_i the eigenvalues of the covariance matrix $C = \frac{1}{K}XX^T$ (the symbol T represents the transposition). As a consequence, the trajectory matrix X is decomposed into a sum of rank-one matrices X_i, $X = \sum_{i=1}^{M} X_i = \sum_{i=1}^{M} \sigma_i u_i v_i^T$, where σ_i, u_i and v_i denote the i^{th} singular value of matrix X, the i^{th} column of matrix U and the i^{th} column of matrix V, respectively.

Reconstruction

In the SSD, the j^{th} component series $g^{(j)}(n)$ is constructed as follows.

(1) At the first iteration, if the test for a sizable trend is positive, only the first left and the first right eigenvectors are employed for generation of $g^{(1)}(n)$, where $g^{(1)}(n)$ is achieved by diagonal averaging of $X_1 = \sigma_1 u_1 v_1^T$.

(2) Otherwise, for iteration $j > 1$, frequency contents of the component series $g^{(j)}(n)$ are congregated in the frequency band $[f_{\max} - \delta f, f_{\max} + \delta f]$, where δf indicates half the width of the dominant peak in the PSD of the residual $v_j(n)$. Consequently, a subset $I_j = (\{i_1, ..., i_p\})$ is grouped from all eigentriples (σ_i, u_i, v_i) whose left eigenvectors demonstrate a dominant frequency in the range $[f_{\max} - \delta f, f_{\max} + \delta f]$ and one of the eigentriples makes the most contributions to the energy of the dominant peak of the selected scales. Accordingly, the j^{th} component series $g^{(j)}(n)$ is retrieved by diagonal averaging of the matrix $X_{I_j} = X_{i_1} + ... + X_{i_p}$ along the cross-diagonals.

Moreover, a spectral model for describing a profile of the PSD is constructed for estimating the dominant peak width δf. Specifically, the model is designed as a sum of three Gaussian functions, each with a spectral peak

$$\gamma(f, \theta) = \sum_{i=1}^{3} A_i e^{-\frac{(f-u_i)^2}{2\sigma_i^2}}, \tag{3}$$

where the parameters A_i, σ_i and u_i symbolize the magnitude, the width and the location of the i^{th} Gaussian function, respectively. Here, $\theta = (A \quad \sigma)^T$, $A = [A_1, \quad A_2, \quad A_3]$ and $\sigma = [\sigma_1, \quad \sigma_2, \quad \sigma_3]$. Afterwards, an optimizing procedure is used to fit the whole PSD. Here, the initial parameters are set as

$$\begin{cases} A_1^{(0)} = \frac{1}{2} PSD(f_{\max}) \\ \sigma_1^{(0)} = f : PSD(f) = \frac{2}{3} PSD(f_{\max}) \end{cases}$$
$$\begin{cases} A_2^{(0)} = \frac{1}{2} PSD(f_2) \\ \sigma_2^{(0)} = f : PSD(f) = \frac{2}{3} PSD(f_2) \end{cases} . \tag{4}$$
$$\begin{cases} A_3^{(0)} = \frac{1}{4} PSD(f_3) \\ \sigma_3^{(0)} = 4|f_{\max} - f_2| \end{cases}$$

This paper determines the optimal values using the Levenberg-Marquardt algorithm, which is a nonlinear minimization algorithm. In case the optimal value is estimated as σ_1, a value for δf is determined as $\delta f = 2.5\sigma_1$. Here, the choice of the factor 2.5 allows almost 99% of the region to be covered by the dominant peak to be accounted for, by leaving the baseline noise out at the same time.

Advantages of the former reconstructing strategy for X_{I_j} lie in unnecessaries to identify the leading eigenvalues relative to the noise floor (or to estimate the rank r of the trajectory matrix). Therefore, the components characterizing scales different from those at iteration j are automatically excluded at iteration j and will be retrieved in the following iterations, because their frequency contents are outside $[f_{\max} - \delta f, f_{\max} + \delta f]$. Underlying the principle is the idea that at each iteration SSD selects the oscillation contributing most of energy in the residual, on the assumption that SSA searches for the frequency bands mostly concentrating the explained energy.

In addition, a second run of the algorithm is performed on the j^{th} component just extracted, $g_{[1]}^{(j)}(n)$ (for $j = 1$, this algorithm is carried out again in case no sizable trend is detected) for improving the results in the first run.

In the end, a scaling factor a is adopted to adjust the variance of $g^{(j)}(n)$ to the residual series $v^{(j)}(n)$, $\hat{a} = \min_a \left\| v^{(j)}(n) - a g^{(j)}(n) \right\|_2^2$, $a = \frac{g^T v}{g^T g}$ and $\tilde{g}^{(j)}(n) = a g^{(j)}(n)$.

Stopping Criterion

In the SSD, a normalized mean square error (NMSE) between the residual and the original signal serves as a stopping criterion. For this reason, the decomposition process will be stopped when the stopping criterion NMSE is less than a given threshold (usually 0.1%).

$$NMSE^{(j)} = \frac{\sum_{i=1}^{N}\left[v^{(j+1)}(i)\right]^2}{\sum_{i=1}^{N}\left[x(i)\right]^2} \quad (5)$$

Finally, the original series $x(n)$ is decomposed into a sum of components and a trend

$$x(n) = \sum_{k=1}^{m} \widehat{g}^{(k)}(n) + v^{(m+1)}(n), \quad (6)$$

where $\widehat{g}^{(k)}(n)$ stands for the k^{th} component, m for the number of retrieved components and $v^{(m+1)}(n)$ for the final trend.

APPLICATION OF SSD TO FAULT FEATURE ENHANCEMENT OF ROLLING BEARINGS

Numerical Verification

A constructed signal containing impulses, noise and trends, mixed with intermittent contents, was for simulating vibrations of a defective rolling bearing. Herein, the addition of the intermittence is simply to increase complexities of the simulated signal. Following this, the simulated signal consists of four components: the impulse component c_1, the intermittent component c_2, the sinusoidal component c_3 and the trend c_4, in addition to the white noise wn. The simulated signal with the length $N = 8000$ and the sample frequency $F_s = 8000$ is expressed as follows

$$x = c_1 + c_2 + c_3 + c_4 + wn, \quad (7)$$

where

$$\begin{cases} c_1 = \sum_{j=1}^{k} c_{1j},\ k = 80 \\ c_{1j} = 0.1\sin\left\{3000\pi\left[t-(0.004+0.0125j)\right]\right\} \cdot \\ \qquad \exp\left\{-600\left[t-(0.004+0.0125j)\right]\right\} \\ t = \dfrac{n}{F_s}, \quad 0 \le n \le N-1 \end{cases}$$

$$c_2 = \begin{cases} \begin{cases} 0.25\sin\left(200\pi t + \dfrac{3\pi}{4}\right) \\ t = \dfrac{n}{F_s}, \quad \dfrac{N}{2} \le n \le N-1 \end{cases} \\ \begin{cases} 0 \\ 0 \le n < \dfrac{N}{2} - 1 \end{cases} \end{cases}$$

$$\begin{cases} c_3 = 0.3\sin\left(46\pi t + \dfrac{\pi}{8}\right) \\ t = \dfrac{n}{F_s}, \quad 0 \le n \le N-1 \end{cases}$$

$$c_4 = 0.2t, \quad t = \frac{n}{F_s}, \quad 0 \le n \le N-1$$

$$wn = 0.01 \cdot std(c_1) \cdot randn(1, N).$$

Here, the symbols $std(\cdot)$ and $randn(1, N)$ mean to calculate the standard deviation and to generate Gaussian white noise with the length N, respectively. The simulated signal x is exhibited in Figure 1 and its four realistic components in Figure 2.

Firstly, EMD was employed to investigate the simulated signal and the results are demonstrated in Figure 3. As demonstrated in Fig. 3, the results from EMD demonstrate severe mode mixing. Afterwards, EEMD was applied to analyze the simulated signal and the results are suggested in Figure 4. According to the suggestion given by Wu, Z.H. and Huang, N.E. (Wu, Z.H. and Huang, N.E., 2009), the amplitude of the added white noise was set as 0.2 time the standard deviation of the simulated signal and the ensemble number as 100 in this paper. As suggested in Fig. 4, the ensemble strategy seemingly fails to allow EEMD to avoid mode mixing. Furthermore, SSD was exploited to examine the simulated signal and the results are illustrated in Figure 5. As a result, Fig. 5 indicates that SSD shows the potential for recovering all the physically interpretative components from the simulated signal.

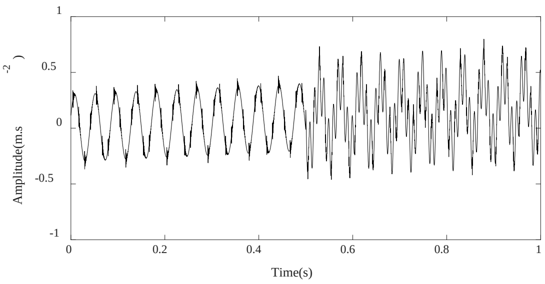

Fig. 1. A simulated signal containing noise, impulses and trends, mixed with intermittent contents.

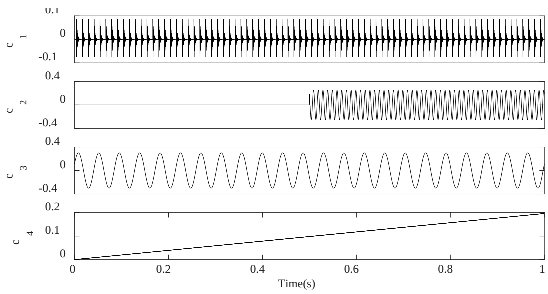

Fig. 2. Four realistic components of the simulated signal.

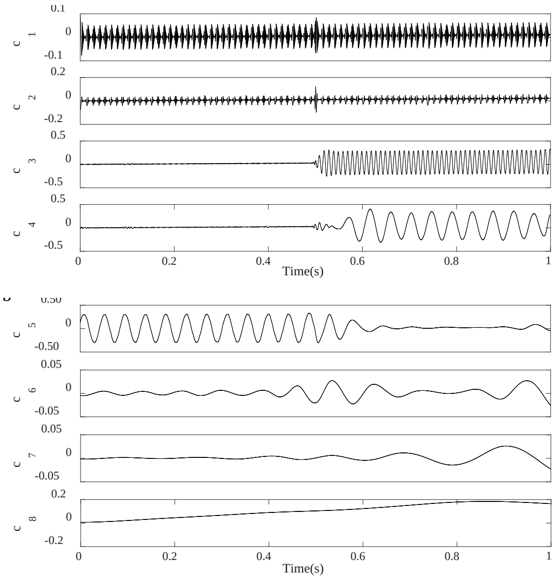

Fig. 3. Decomposition results of the simulated signal using EMD, (a) the 1^{st}~4^{th} components, (b) the 5^{th}~8^{th} components.

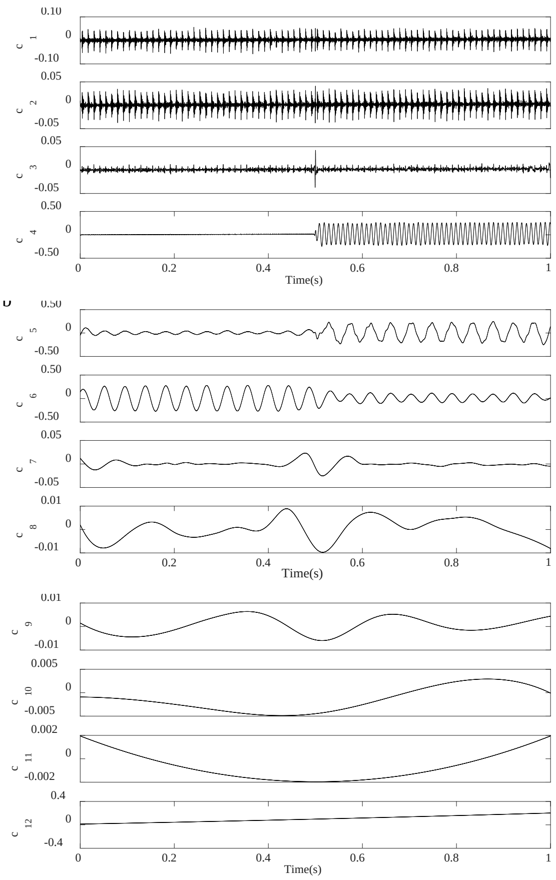

Fig. 4. Decomposition results of the simulated signal using EEMD, (a) the 1^{st}~4^{th} components, (b) the 5^{th}~8^{th} components, (c) the 9^{th}~12^{th} components.

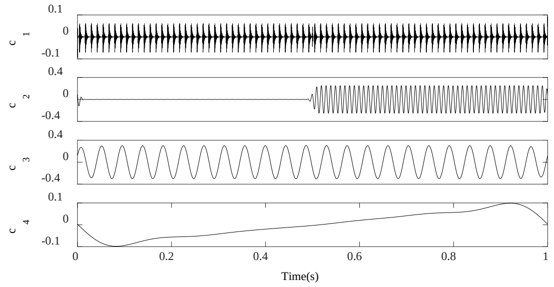

Fig. 5. Decomposition results of the simulated signal using SSD.

Case Study

In this subsection, the performance of SSD was further benchmarked against each of envelope analysis, EMD and EEMD using realistic rolling-bearing fault data from Case Western Reserve University Bearing Data Center (Bearing Data Center Website, Case Western Reserve University). These accelerating vibration data of bearings contain single-point faults introduced by electro-discharge machining. The bearing vibration data were collected from drive end bearings, which are SKF 6205-2RS deep groove ball bearings, with the sample frequency 12000Hz and the size 12000. Table 1 displays defect frequencies of the rolling bearing.

Fault Diagnosis of Bearing Inner Races

A piece of bearing inner-race fault data with the running speed about 1418 RPM was manifested in Figure 6. According to Table 1, the defect frequencies for inner races, outer races, cage train and rolling elements are about 128Hz, 85Hz, 9.4Hz and 111Hz, respectively. Firstly, envelope analysis was employed to research the bearing inner-race fault data and the results are demonstrated in Figure 7. As demonstrated in Fig. 7, the frequencies 128Hz and 110Hz almost match the defective frequencies of inner rings and rolling elements, respectively. As a consequence, an obvious clue to the identity of the bearing fault type is hard to find from the envelope spectra. In the following, EMD was used to analyze these inner-race fault data and the results are suggested in Figure 8, which is composed of twelve components. By trial and error, the first three components, which contain most of useful information, were selected for further analysis. Envelope spectra of the first three components recovered by EMD are displayed in Figure 9. Here, Fig. 9(b) seemingly demonstrates inner-race fault characteristics, since the frequencies 254Hz and 381Hz are near the first- and second-order harmonics of the inner-race defective frequency, respectively. However, the frequency 110Hz is so near to the defect frequency of the rolling element that it causes incorrect identification of the bearing fault type, still occurring in Fig. 9(b). Afterwards, EEMD was applied to examine these inner-race fault data and the results are revealed in Figure 10, which contains twelve components. Also, envelope spectra of the first three components retrieved by EEMD are displayed in Figure 11. It turns out that Fig. 11(b) exhibits the defect frequency of the inner races and the first two harmonics thereof. Nevertheless, the spectra in Fig. 11(b) are still contaminated by the frequency 110Hz. Moreover, SSD was adopted to examine the inner-race fault data and the results are suggested in Figure 12. As suggested in Fig. 12, SSD decomposes the inner-race fault data into just four components. Figure 13 shows envelope spectra of the first three components recovered by SSD. Consequently, Fig. 13(c) gives a more successful exhibition of the inner-race defective characteristics, in contrast with either of Fig. 9 and Fig. 11.

Table 1. Defect frequencies of the rolling bearings (Multiple of running speed in Hz).

Inner Race	Outer Race	Cage Train	Rolling Element
5.4152	3.5848	0.39828	4.7135

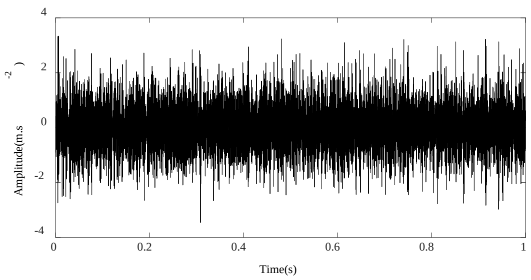

Fig. 6. A piece of bearing inner-race fault data.

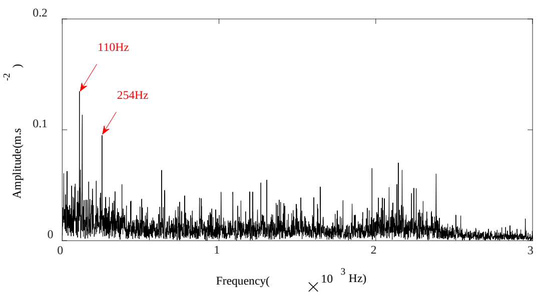

Fig. 7. Envelope spectra of the bearing inner-race fault data.

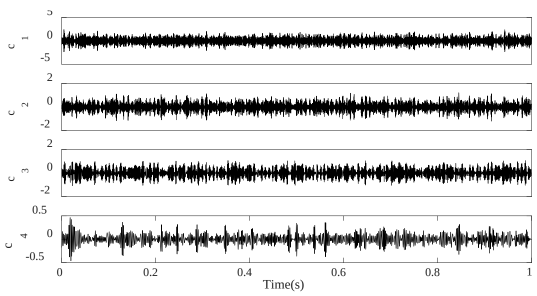

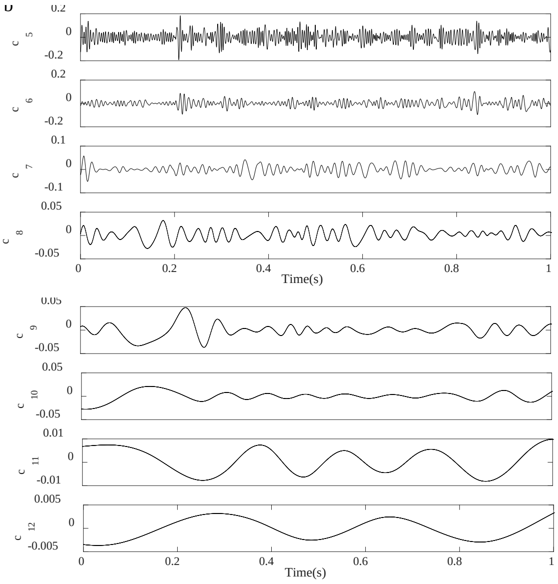

Fig. 8. Decomposition results of the bearing inner-race fault data using EMD, (a) the 1^{st}~4^{th} components, (b) the 5^{th}~8^{th} components, (c) the 9^{th}~12^{th} components.

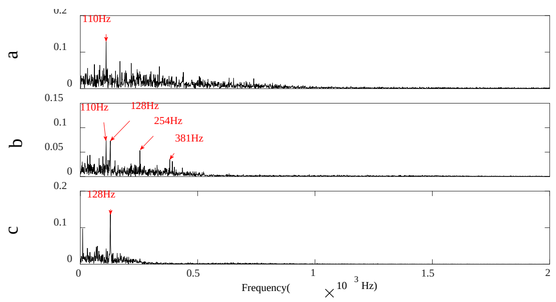

Fig. 9. Envelope spectra of the first three components retrieved by EMD, (a), (b) and (c) represent envelope spectra of the first, the second and the third component, respectively.

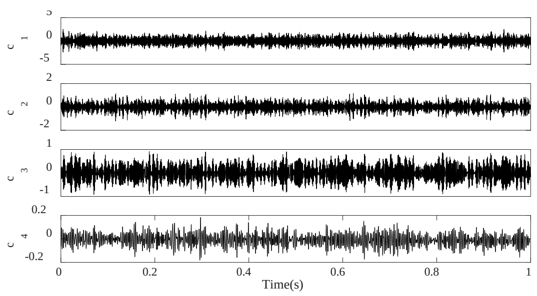

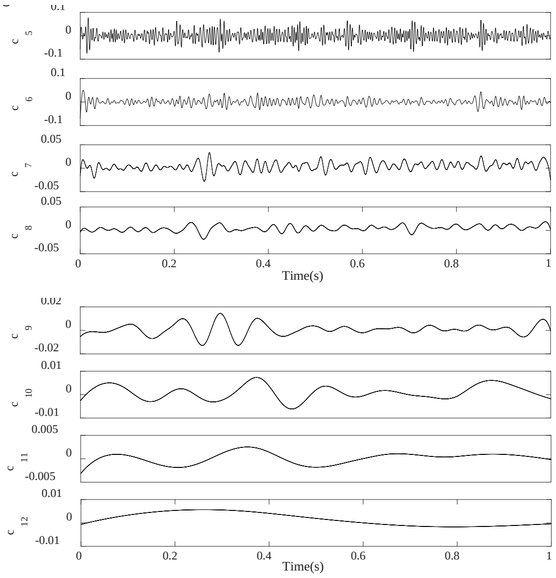

Fig. 10. Decomposition results of the bearing inner-race fault data using EEMD, (a) the 1st~4th components, (b) the 5th~8th components, (c) the 9th~12th components.

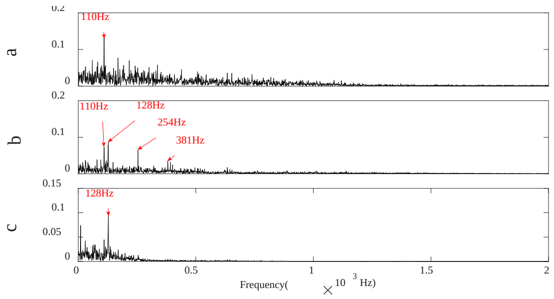

Fig. 11. Envelope spectra of the first three components retrieved by EEMD, (a), (b) and (c) represent envelope spectra of the first, the second and the third component, respectively.

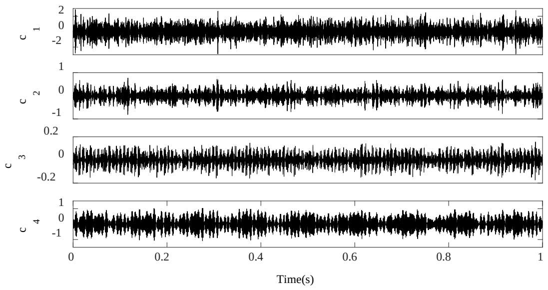

Fig. 12. Decomposition results of the bearing inner-race fault data using SSD

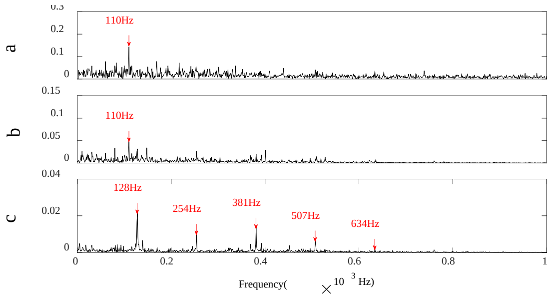

Fig. 13. Envelope spectra of the first three components retrieved by SSD, (a), (b) and (c) represent envelope spectra of the first, the second and the third component, respectively.

Fault Diagnosis of Bearing Outer Races

Afterwards, the performance of SSD was further measured using bearing outer-race fault data. Figure 14 describes a piece of bearing outer-race fault data with the running speed 1773RPM. Hence, the defect frequencies for inner races, outer races, cage train and rolling elements are about 160Hz, 106Hz, 11.8Hz and 139Hz, respectively. Envelope spectra of the outer-race fault data are depicted in Figure 15. Because the frequencies 109Hz, 216Hz and 324Hz are close to the defect characteristics of the bearing outer race, the second-order and the third-order harmonics thereof, respectively, Fig. 15 seems to give a display of bearing outer-race characteristics to some extent. Nonetheless, as shown in Fig. 15, some frequencies, such as the frequency 157Hz, cause a disturbance to identification of bearing fault types. Then, EMD was made use of exploring these outer-race fault data and the results are exhibited in Figure 16, which consists of eleven components. By trial and error, the first component, which incorporates most of useful information, was chosen for analysis. Figure 17 shows envelope spectra of the first component recovered by EMD. Nonetheless, compared with Fig. 15, Fig. 17 does not demonstrate a significant improvement in highlighting the defect frequencies. Moreover, EEMD was used to probe these outer-race fault data and the results are displayed in Figure 18, which comprises twelve components. Figure 19 describes envelope spectra of the first component recovered by EEMD. However, compared with Fig. 15, Fig. 19 is still unsuccessful in showing an improvement in highlighting the defect frequencies. In addition, SSD was applied to investigate these outer-race fault data and the results are displayed in Figure 20, which consists of five components. Envelope spectra of the first component retrieved by SSD are depicted in Figure 21. Compared with each of Fig. 15, 17 and 19, Fig. 21 more significantly highlights the defect frequencies.

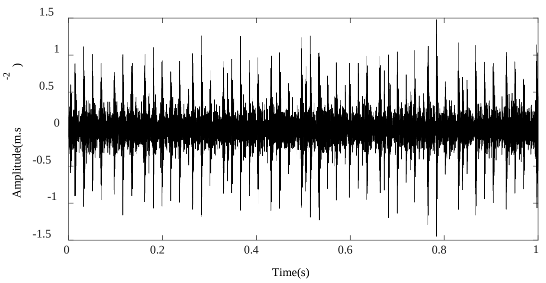

Fig. 14. A piece of bearing outer-race fault data.

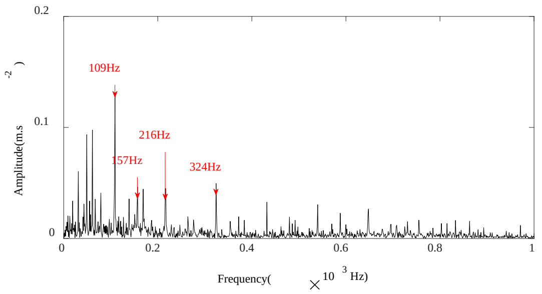

Fig. 15. Envelope spectra of bearing outer-race fault data.

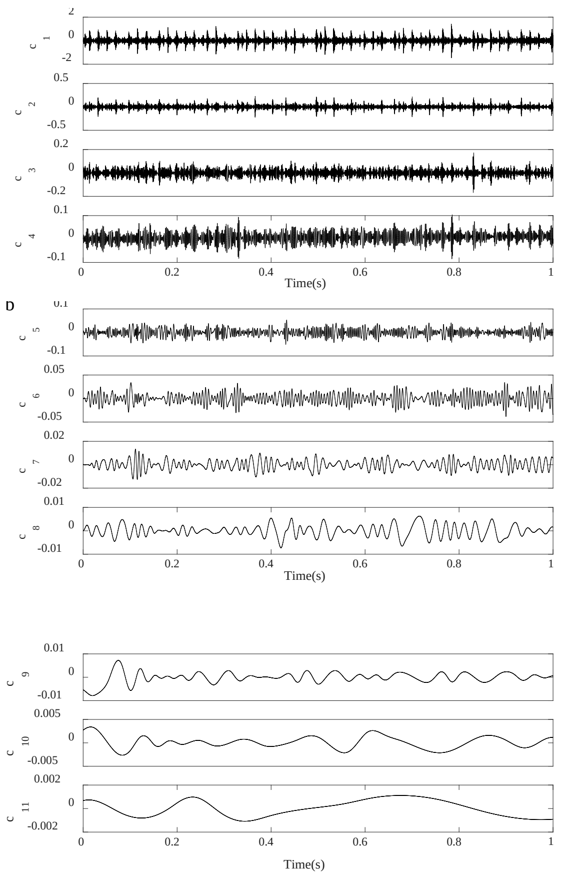

Fig. 16. Decomposition results of bearing outer-race fault data using EMD, (a) the 1st~4th components, (b) the 5th~8th components, (c) the 9th~11th components.

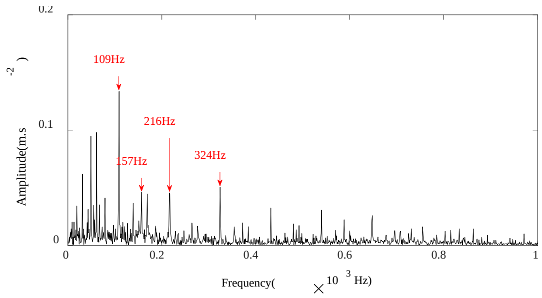

Fig. 17. Envelope spectra of the first component retrieved by EMD.

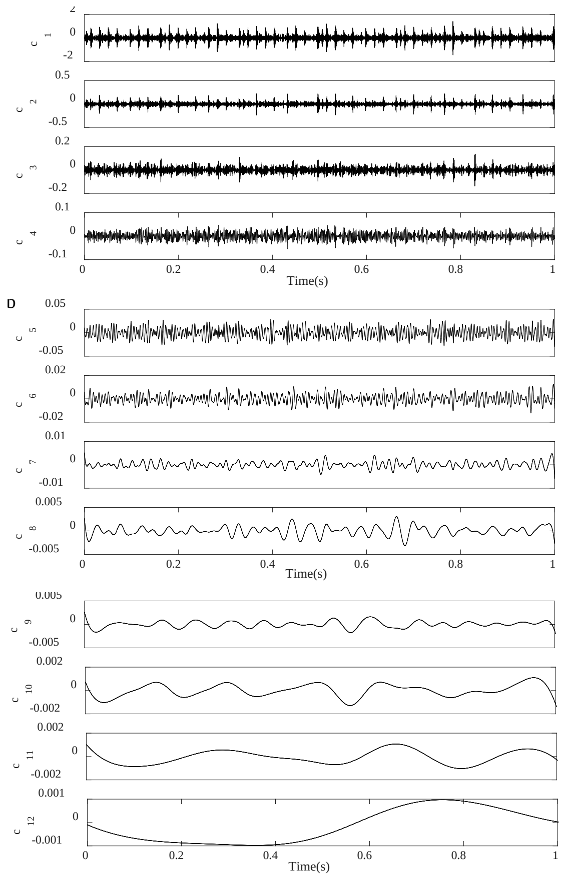

Fig. 18. Decomposition results of bearing outer-race fault data using EEMD, (a) the 1st~4th components, (b) the 5th~8th components, (c) the 9th~12th components.

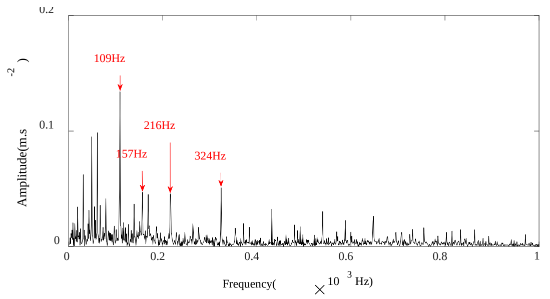

Fig. 19. Envelope spectra of the first component retrieved by EEMD.

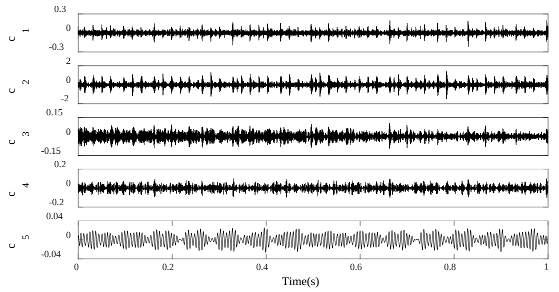

Fig. 20. Decomposition results of bearing outer-race fault data using SSD.

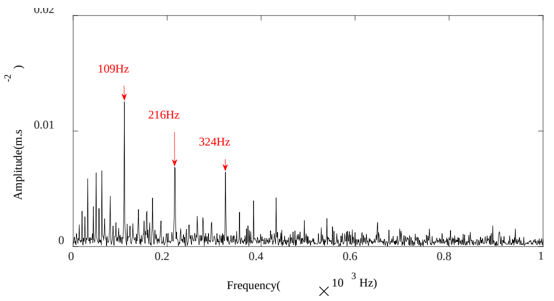

Fig. 21. Envelope spectra of the first component retrieved by SSD.

DISCUSSIONS

Although either of SSD and EMD can serve to examine nonstationary and nonlinear data, there is a considerable difference between them both. EMD extracts components from original data in descending order of frequencies. Since lacking focuses on practically physical meaning of components, EMD inevitably yields mode mixing. By contrast, SSD extracts components from original data in descending order of energy of spectral peaks. Owing to protecting natural properties of spectral peaks at utmost, SSD can generate components with clear physical meaning by effectively restraining mode mixing.

Although feasible in feature enhancement of complex vibration data, SSD still suffers from some difficulties, such as identification and separation of the trend, evaluation of proprieties of the default value 1% of the original variance and the end effects from spurious oscillations describing the edge of the reconstructed SSD-components. These problems require further study in future.

CONCLUSIONS

This paper introduced SSD to examine complex bearing vibration data and proposed a novel method for fault feature enhancement of bearings based on SSD. Both numerical and experimental examples confirmed the feasibility of the proposed method. Additionally, the comparison of SSD with envelope analysis, EMD and EEMD indicates that SSD outperforms the other methods in enhancing fault features of bearings as well as restraining mode mixing.

ACKNOWLEDGEMENTS

The authors would like to kindly thank Bearing Data Center of Case Western Reserve University for providing rolling bearing fault data. The work was supported by Shandong Provincial Natural Science Foundation China (ZR2012EEL07, ZR2014EEP015).

REFERENCES

Bearing Data Center Website, Case Western Reserve University.

Bonizzi, P., KAREL, J.M., Meste, O. and Peeters, R.L., "Singular spectrum decomposition: A new method for time series decomposition", Adv. Adapt. Data Anal., Vol. 6, No. 4, pp. 1-29(2014).

Daubechies, I., Ten Lectures On Wavelets, Springer-Verlag, Berlin, pp. 1-16(1992).

Huang, N.E., Shen, Z., Long, S.R., Wu, M.L.C., Shih, H.H., Zheng, Q.N., Yen, N.C., Tung, C.C. and Liu, H.H., "The empirical mode decomposition and the Hilbert spectrum for nonlinear and non-stationary time series analysis ", P. Roy. Soc. Lond. A Mat., Vol. 454, No. 1971, pp. 903-995(1998).

Lin, J., "Improved Ensemble Empirical Mode Decomposition and its Applications to Gearbox Fault Signal Processing", Int. J. Comput. Sci. Issues, Vol. 9, No. 6, pp. 194-199(2012).

Vautard, R. and Ghil, M., "Singular spectrum analysis in nonlinear dynamics, with applications to paleoclimatic time series", Physica D, Vol. 35, No. 3, pp. 395-424(1989).

Vautard, R., Yiou, P. and Ghil, M., "Singular-spectrum analysis: A toolkit for short, noisy chaotic signals", Physica D, Vol. 58, No. 1-4, pp. 95-126(1992).

Wu, Z.H. and Huang, N.E., "Ensemble empirical mode decomposition: a noise-assisted data analysis method", Adv. Adapt. Data Anal., Vol. 1, No. 1, pp.1-41(2009).

Zhang, J., Yan, R., Gao, R.X. and Feng, Z., " Performance enhancement of ensemble empirical mode decomposition", Mech. Syst. Signal Process., Vol. 24, No.7, pp. 2104-2123(2010).

基於奇異譜分解的滾動軸承故障特徵增強

竇春紅　魏學業　張俊紅　胡良
北京交通大學電子資訊工程學院

摘 要

滾動軸承的故障特徵通常比較微弱。因此，滾動軸承的故障診斷具有挑戰性。基於平穩性和線性理論的傳統資料分析方法不適合處理軸承振動資料。EMD 和 EEMD 方法雖然被用於處理非平穩和非線性信號，但是這兩個方法存在著模態混疊問題。為此，本文將一種新的信號處理方法—奇異譜分解(Singular Spectrum Decomposition, SSD)用於分析軸承故障信號，提出了一種基於 SSD 的軸承故障特徵增強方法。接著，將本文所提出的方法與包絡分析、EMD 和 EEMD 方法進行了比較，結果表明本文所提出的方法在抑制模態混疊及提取具有物理意義的信號分量方面具有優勢，在增強軸承故障特徵方面具有潛力。